GPS Solut (2012) 16:231–241
DOI 10.1007/s10291-011-0225-9

ORIGINAL ARTICLE

Altimetry with GNSS-R interferometry: first proof of concept experiment

Antonio Rius · Oleguer Nogués-Correig · Serni Ribó · Estel Cardellach · Santi Oliveras · Enric Valencia · Hyuk Park · José Miguel Tarongí · Adriano Camps · Hans van der Marel · Roel van Bree · Bas Altena · Manuel Martín-Neira

Received: 14 December 2010 / Accepted: 2 May 2011 / Published online: 17 June 2011

Abstract The Global Navigation Satellite System Reflectometry (GNSS-R) concept was conceived as a means to densify radar altimeter measurements of the sea surface. Until now, the GNSS-R concept relied on open access to GNSS transmitted codes. Recently, it has been proposed that the ranging capability of the technique for ocean altimetric applications can be improved by using all the signals transmitted in the bandwidth allocated to GNSS, which includes open access as well as encrypted signals. The main objective of this study is to provide experimental proof of this enhancement through a 2-day experiment on the Zeeland Bridge (The Netherlands). In the experiment, we used a custom built GNSS-R system, composed of high gain GPS antennas, calibration subsystem, and an FPGA-based signal processor which implemented the new concepts, an X-band radar altimeter and a local geodetic network. The results obtained indicate that the new approach produces a significant improvement in GNSS-R altimetric performance.

Keywords Ocean altimetry · GNSS reflectometry · Bistatic radars

A. Rius (✉) · O. Nogués-Correig · S. Ribó · E. Cardellach · S. Oliveras
Institut d'Estudis Espacials de Catalunya-CSIC, Campus UAB, Fac. Ciencias, Torre C5 parell 2, 08193 Bellaterra, Spain
e-mail: rius@ieec.uab.es

E. Valencia · H. Park · J. M. Tarongí · A. Camps
Institut d'Estudis Espacials de Catalunya-UPC, Campus Nord, Jordi Girona 1-3, 08034 Barcelona, Spain

H. van der Marel · R. van Bree · B. Altena
Institute of Earth Observation and Space Systems, Faculty of Aerospace Engineering, Delft University of Technology, Kluyverweg 1, 2629 HS Delft, The Netherlands

M. Martín-Neira
European Space Research and Technology Centre, Keplerlaan 1, 2200 AG Noordwijk, The Netherlands

Introduction

Space borne bistatic radars using opportunity signals reflected onto the earth's surface were proposed in Martín-Neira (1993) to densify, in time and space, the mean sea level measurements provided by monostatic radar altimeters. This concept was described in terms of the measurements of the coherence of the direct and reflected signals, obtained using radiointerferometric techniques, and was termed the Passive Reflectometry and Interferometry System (PARIS). A detailed description of such radiointerferometric techniques and references to related applications, such as sea interferometry and moon reflectometry, can be found in Thompson et al. (2004).

When the sources of opportunity are the GNSS, the PARIS concept is called GNSS-Reflectometry (GNSS-R). In such a case, because the information to create some of the components of the transmitted signals is available, we could cross-correlate the reflected signals with their modeled replicas. Successful detection of GNSS-R signals from space has been reported in Lowe et al. (2002) and Gleason et al. (2005), after the cross-correlation of the reflected signals with their modeled replicas.

With this standard approach, GNSS-R ignores the encrypted components of the signals, collects less power in narrower bandwidth, and thus lowers the achievable performance of the technique. To overcome this limitation, the European Space Agency (ESA) has announced the PARIS

In-Orbit Demonstrator (PARIS-IOD) space mission, as described in Martín-Neira et al. (2011), based on the cross-correlations of GNSS signals collected with two high gain antennas. In this paper, we will use the term GNSS-Ri to denote this *interferometric* approach.

An additional advantage of GNSS-Ri is that it is not sensitive to distortions in the transmitted signals. In the GNSS-R implementations, the modeled replicas differ slightly from the actual transmitted signals. This will distort the shape of the measured cross-correlations and will produce SNR losses and uncertainties in the delay measurements, inducing errors in the altimetric information sought. See a recent discussion in Wong et al. (2010), and in the references cited there, describing such deformations and showing that they are common.

We present the first GNSS-Ri proof of concept experiment performed to demonstrate the feasibility of the technique by sensing the sea tide from a bridge in the Netherlands. In the following sections, we describe the setup used to gather GNSS-Ri data and the waveform models developed to derive the altimetric information from the observations. Finally, we compare our results with the mean sea level estimates obtained from independent X-band radar altimeter measurements performed simultaneously.

Experiment setup

On July 7 and 8, 2010, in two sessions from 10:00 to 18:00 UTC (hereafter, Sessions A and B), we deployed on the Zealand Bridge (The Netherlands) a system composed of (a) a custom GNSS-Ri observational system, (b) an X-band radar altimeter (XBRA), and (c) a local geodetic network, to tie (a) and (b). The setup is shown in Fig. 1.

GNSS-Ri observational system

The GNSS-Ri system deployed at the Zeeland Bridge was composed of:

- Two fixed GPS L1-band directional antennas, U (up looking) and D (down looking), mounted at the end of a 4 m boom over the sea, with boresights (Azimuth, Elevation) equal to (310°, 70°) and (310°, −70°). This pointing was the result of a careful a priori study, which maximized for the experiment site and date the number of hours per day for which only one GPS space vehicle (SV) would pass through the antenna's main beam, leaving the rest of satellites away from the main beam with a relative strength with respect to the radiation pattern peak of −15 dB at most. This amounted to about 2 h per day. The output of these U and D antennas is a pair of signals (Y_d, Y_r), where the subscripts d and r stand for direct and reflected, respectively.
- A two-position switch, controlled by the PARIS Interferometric Receiver (PIR) rack, delivers the signal pair (Y_x, Y_y), equal to (Y_d, Y_r) or (Y_r, Y_d) depending on the switch position. This makes it possible to swap the antenna outputs as inputs of the receiver.
- The PIR-signal processor (PIR-SP), placed inside the PIR rack, computes in real time the GNSS-Ri complex cross-correlations $\mathbf{Z_{xy}}$ defined in Eq. 1, where ($\mathbf{Y_x}$, $\mathbf{Y_y}$) is the analytic representation of the real signals (Y_x, Y_y). These waveforms are sent and stored in real time to a laptop computer, not depicted in Fig. 1, which is external to the PIR rack.
- A GPS receiver inside the PIR rack, not depicted in Fig. 1, provides the GPS time frame reference using the signals captured by the GPS antenna N.

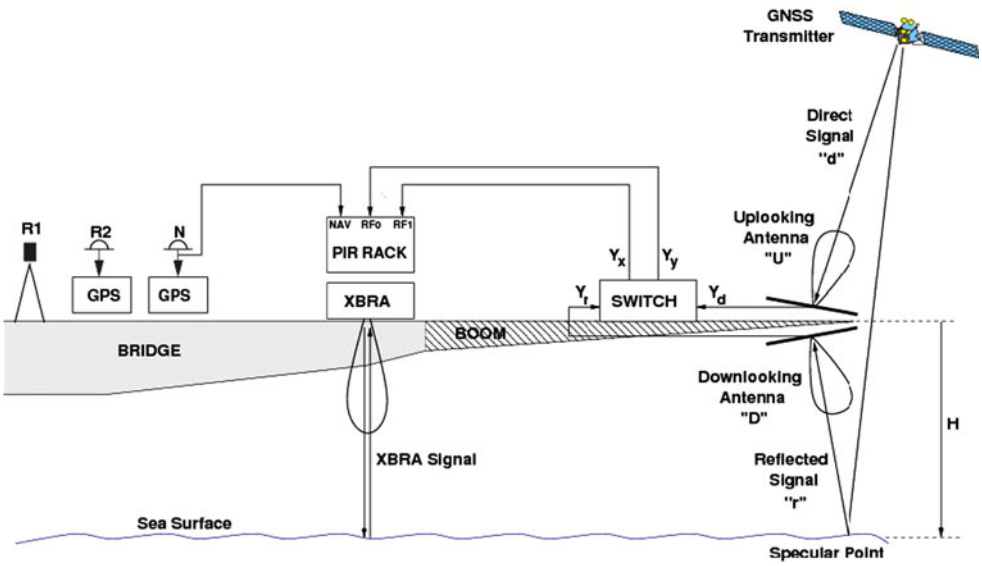

Fig. 1 Logical arrangement of the Zealand Bridge setup. The system produced two independent measurements of the mean sea level *H*. It is composed of a GNSS-Ri Instrument, and an X-band radar altimeter (XBRA). A local reference frame was established using a TOPCON GPT-7003i Total Station (R1), and a GPS reference point (R2). The hemispherical antenna of a GPS receiver (N) was used to provide time reference to the PIR rack

The relevant parameters of the GNSS-Ri instrument are summarized in Table 1. Antennas only differ in terms of polarization, U was RHCP and D was LHCP. The gain was 6 dB lower than the directivity, due to the fact that the antenna had an ohmic efficiency of 0.25.

The main parts of the PARIS Interferometric Receiver are presented in Fig. 2. It is composed of the RF calibration switch, the down conversion chains, and the signal processor, which includes a 320-lag complex correlator with a sampling rate of $F_s = 80$ MHz, continuously delivering the complex correlations:

$$\mathbf{Z_{xy}}(t,\tau)\Big|_{\tau=m\cdot T_s} = \int_{u=-T_c/2}^{u=+T_c/2} \mathbf{Y_x}(t+u)\mathbf{Y_y^*}(t+u-\tau)\mathrm{d}u\Big|_{\tau=m\cdot T_s} \quad (1)$$

with $m \in [80, 239]$ and $T_s \equiv 1/F_s = 12.5$ ns. The correlation channel works with a fixed coherent integration time of $T_c = 1$ ms. The waveforms are sent in real time to the PIR laptop through the Ethernet link and saved. The cross-correlation function has a different meaning depending on the switch position, as commented previously. The PIR-SP is autonomous and does not receive any command from outside. The PIR-signal processor works on a sequence basis that repeats every GPS minute and controls the switch position. The GPS receiver inside the PIR rack provides the GPS time frame to the PIR-SP via a signal of one pulse per second (1 PPS) and time data logs that are synchronized with this 1PPS, which provide the GPS time tags in a *week* and *second-of-week* format. The GPS receiver clock is totally independent and incoherent with respect to the PIR rack 30 MHz reference clock. The downconverters are locked to that reference in order to generate their internal LO tones coherently. Also, the PIR-SP takes that clock reference and internally boosts it up to 80 MHz to generate its own working clock. We chose a 30 MHz clock reference because the 52nd and 53rd harmonics of this frequency fall at ±15 MHz around the GPS L1 carrier, avoiding the instrument self-interference inside the band that we experienced with a 20 MHz reference in our preliminary prototype designs of the receiver. Any tone added to the input signals in both correlator inputs contributes to the cross-correlation, while in the normal GNSS receiver, the signal is correlated with a model, removing this effect of the interference through the correlation process.

Table 1 GNSS-Ri system parameters

Parameter	Value	Parameter	Value
U/D antenna directivity	15 dBi	U/D antenna gain	9 dBi
U polarization	RHCP	D polarization	LHCP
Sidelobes	<−35 dB	Switching rate	1 Hz
Sampling rate	80 MHz	RF signal bandwidth	24 MHz

X-band radar altimeter

The X-band radar altimeter (XBRA) is a *WaveGuide* short range FMCW radar produced commercially by RADAC BV of The Netherlands. The radar operates in the 9.8–10.3 GHz frequency range and has a distance range of 1–75 m. The width of the radar beam is about 5°. The X-band radar measures the distance to the water surface, or heave, at a rate of 2.56 samples per second (391 ms interval). The height of the water level, significant wave height (SWH) and wave period, as well as several other parameters including energy density spectra, were computed from the raw heave (height) measurements. We found that SWH was in the order of 10 cm during both sessions.

The standard deviation of the raw heave data, computed from the first differences, was 4.12 cm for July 7 and 4.58 cm for July 8. These standard deviations include, besides measurement errors, the high frequency part of the waves. Normalized to 1 s, the precision of the heave data is better than 2.9 cm. In order to eliminate the effects of

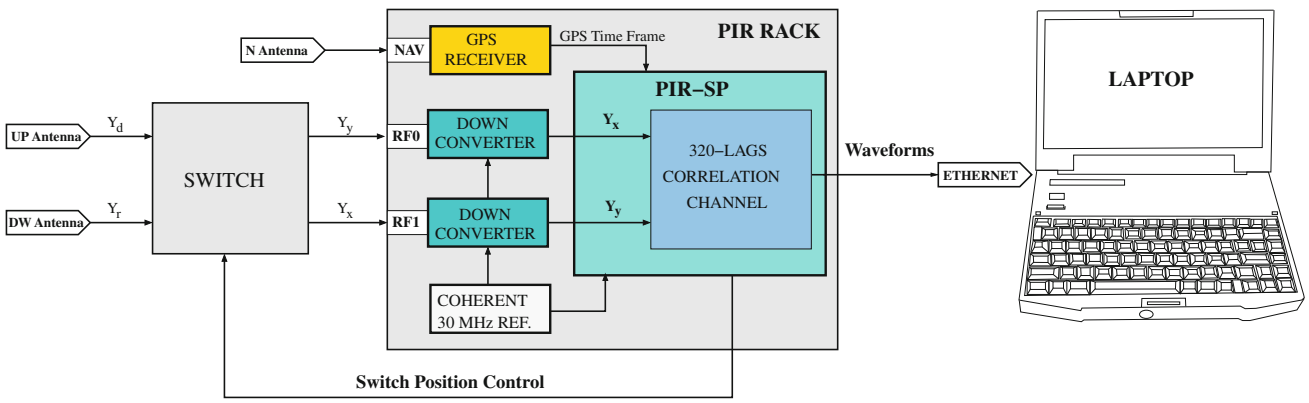

Fig. 2 PIR receiver parts: the switch, the rack and the laptop

waves, the raw heave data have been smoothed. We have compared 10-min averages with 1 min averages and 10-s averages. The standard deviation of the differences with the 10 min smoothed data was about 0.5 cm for the 1 min smoothed data and less than 1 cm for the 10-s smoothed data. As a reference for the GNSS-Ri, we have selected the 10 min average sea level height $H10$, which is recorded at 1 min intervals. It is estimated that the sea-level height $H10$ is precise to less than 1 cm.

The X-band radar data have been compared with tide gauge data from two nearby tide gauges at distances of 7.4 and 15.3 km. The data from these tide gauges have been interpolated to the location of the X-band radar. There is a systematic difference between the interpolated sea level from the tide gauges and the X-band radar of about 1.3 cm with a slow oscillation of an amplitude of about 2 cm. This difference is well within the accuracy of the interpolation. According to the manufacturer's specifications, the bias in the X-band radar should be within a few millimeters. The comparison with the tide gauge data confirms that there are no relevant biases in the X-band radar data.

Local survey measurements

A local survey was carried out on the bridge every 1–2 h to monitor the height differences between the antennas of the GNSS-Ri and the X-band radar, which were mounted 27 m from the GNSS-Ri and to connect these instruments to various stable reference points on the bridge. For the survey, we used a Topcon GPT–7003i Total Station. The precision of the local survey measurements, including the height difference between PIR and WG, were better than 1 mm in height. However, the Total Station measurements revealed that the area of the bridge where the PIR was mounted, including the boom itself, moved by 3 cm in height during the day. The motion of the X-band radar, which was closer to the main pillar, was smaller. The X-band radar data were corrected for the zero-point offset between the X-band and GNSS-Ri ($\sim$16 cm) and the smooth diurnal bridge deformation ($\sim$3 cm), in order to provide a "true" data set for the GNSS-Ri data.

Another part of the local survey measurements consisted of measuring GPS baselines to a nearby height benchmark in the national ordnance datum Normaal Amsterdams Peil (NAP). The GPS measurements were necessary in order to compare data from nearby tide gauges, which are given in the NAP datum, to the X-band radar data. The internal consistency between the completely independent GPS baselines was at the millimeter level. The measurements also showed that reference points of the stable part of the bridge were indeed stable.

Interferometric waveforms model and data analysis

There is a relevant difference between the nature of the waveforms obtained with GNSS-R or GNSS-Ri. In the first case, the reflected signal is correlated with a replica which is associated to a particular transmitter. In the case of GNSS-Ri, this association does not exist, and we need to rely on the discrimination provided by the antenna directivities and the relative delay and Doppler shifts applicable in the correlator. In our experiment, the relative delay was less than twice the height of the bridge ($\sim$18 m), and the relative Doppler shift was negligible due to the static nature of the experiment. Consequently, the discrimination could only be provided by the antenna directivity. We describe the analysis performed with our primary observables, the waveforms, to obtain derived observables like the relative delays.

Signal model

The GNSS-Ri observables are the mean power waveforms. The model used in our implementation is based on Zavorotny and Voronovich (2000), Garrison et al. (2002), and Martín-Neira et al. (2011). The complex $\mathbf{Y_x}$ and $\mathbf{Y_y}$ signals are divided into consecutive coherent integration periods of length $T_c = 1$ ms, to compute the complex cross-correlation $\mathbf{Z_{xy}}$ as defined in Eq. 1. The mean $\langle|\mathbf{Z_{xy}}(t,\tau)|^2\rangle$ computed during an incoherent integration time T_{nc} are the waveforms w_{xy}:

$$w_{xy}(t,\tau) = \frac{1}{T_{nc}} \int_{t-T_{nc}/2}^{t+T_{nc}/2} \langle|\mathbf{Z_{xy}}(t',\tau)|^2\rangle \mathrm{d}t' \tag{2}$$

where t in Eq. 2 is the time tag associated to the incoherent integration interval, and τ is the cross-correlation delay variable, in the range $-1\ \mu s < \tau < 3\ \mu s$ (or $-300 < \tau < 900$ m), sampled at a rate of 80 MHz.Assuming that the complex noise terms in $\mathbf{Y_x}$ and $\mathbf{Y_y}$ are uncorrelated, the waveforms in Eq. 2 are modeled as the sum of signal and noise terms:

$$w_{xy}(t,\tau) = w_s(t,\tau) + w_n(t,\tau) \tag{3}$$

with the signal term is

$$w_s = \sum_{\text{all }:S} w_s^S(t, \tau - \tau_S) \tag{4}$$

where w_s^S is the signal waveform corresponding to satellite S, which according to Zavorotny and Voronovich (2000), Garrison et al. (2002), and Martín-Neira et al. (2011) could be written as:

$$w_s^S(t,\tau) = P_T^S P_{\mathrm{r}}^S(\tau) * |W^S(\tau)|^2 \tag{5}$$

For each transmitter S, P_T^S is the power of the received direct signal, the function $P_r^S(\tau)$ is the average reflected signal power from the sea surface scatterers arriving with a delay τ, and $W^S(\tau)$ is the Woodward Ambiguity Function (WAF) associated to the complex baseband modulation of the signal and * is the convolution operator. The use of Eq. 4 is necessary when the differences between relative delays τ_S for different transmitters are smaller than the width of the WAF function, that is, when the waveforms of different satellites overlap.

If the footprint of the function P_r^S is much smaller than the footprint of $|W^S|^2$ (or $P_r^S \propto \delta$, the Dirac function), as in our experiment, neglecting constant factors and free-space losses, Eq. 5 takes the simple form:

$$w_s^S(t,\tau) = C^S |W^S|^2 \tag{6}$$

with $C^S = \left(P_T^S G_T^S\right)^2 G_{R,\mathrm{d}} G_{R,\mathrm{r}} \sigma$, where $G_{R,\mathrm{d}}$ and $G_{R,\mathrm{r}}$ are the power gain of the transmitter, U and D antennas along the corresponding link path, and σ is a scattering coefficient.

Data analysis

During both sessions, the PIR-SP produced waveforms continuously, repeating each minute a sequence of different calibration switch positions. The data used in this research were collected each minute from seconds 10 through 29; the calibration switch was set to obtain $w_{xy} = w_{\mathrm{dr}}$ for the ten even seconds (10, 12, …, 28) and $w_{xy} = w_{\mathrm{rd}}$ for the ten odd seconds (11, 13, …, 29). Both data sets were integrated independently to have two waveforms each minute with an effective incoherent integration time of 10 s. To simplify the description, we ignore the 1-s difference between the time stamps of the waveforms, assuming that both waveforms $w_{\mathrm{dr}}(t,\tau)$ and $w_{\mathrm{rd}}(t,\tau)$ were obtained at the same time t, and carry the same altimetric information.

The Session B set of waveforms $w_{\mathrm{dr}}(t,\tau)$ is shown in Fig. 3, for delays τ in the interval [−20:100] m. We normalized each waveform by dividing it by its maximum value. A similar aspect is obtained for Session A. Figure 4 shows details of six waveforms extracted from this data set, for delays τ in the interval [−300:350] m, with the same normalization. The M-code component is seen with the highest contrast during the 14:00–15:00 UTC period in both Sessions A and B. We will refer to these 1-h intervals as slices A and B.

We extracted from each waveform w, either w_{dr} or w_{rd}, its maximum value $w^{\max}$, the delay associated with this value τ^{peak}, the pointing waveform delay $\tau^{\mathrm{pointing}} = 0.5(\tau^+ + \tau^-)$, and the waveform width $\beta(t) = \tau^+ - \tau^-$, where $\tau^+ > \tau^-$ are the solutions to the equation $w(t,\tau) = 0.64 w(t,\tau^{\mathrm{peak}})$. The factor 0.64 has been selected to use data with large slopes to increase the sensitivity (Figs. 3, 4). These values are presented in the three lower panels of Fig. 5. With this choice, the width of a 24 MHz filtered WAF containing C/A, P(Y) and M signals, with the power levels given in Barker et al. (2000), is approximately 13.5 m. The upper panel of Fig. 5 shows the XBRA heights $H10(t)$, smoothed with a 10-min sliding window, and referred to the GNSS-Ri reference point. The uncertainty of these 10-min measurements, including instrumental errors, is about 1 cm. According to Fig. 5, Panel 3, within the noise we have $\tau_{\mathrm{dr}}^{\mathrm{peak}}(t) = \tau_{\mathrm{dr}}^{\mathrm{pointing}}(t)$, indicating that the shape of the waveforms is almost unaffected by the scattered power function P_r. The same equality is obtained with the data obtained when the switch was in the other position. These common values will be designated $\tau_{\mathrm{dr}}^{\mathrm{PIR}}(t)$ and $\tau_{\mathrm{rd}}^{\mathrm{PIR}}(t)$, which could be related with an instrument bias

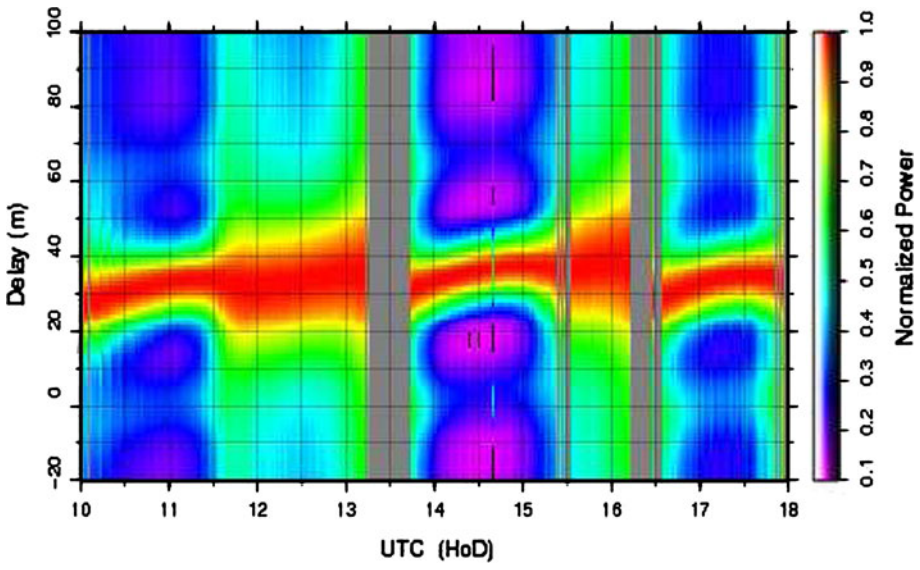

Fig. 3 The normalized waveforms obtained during Session B, represented as a function of cross-correlation delay τ and the UTC). The M-code autocorrelation has a narrower peak than the P(Y) code and has important sidelobes that are approximately 30 m away from the peak. This is visible during intervals including 11:00 UTC, 14:30 UTC and 17:00 UTC. Some of these waveforms are represented in Fig. 4

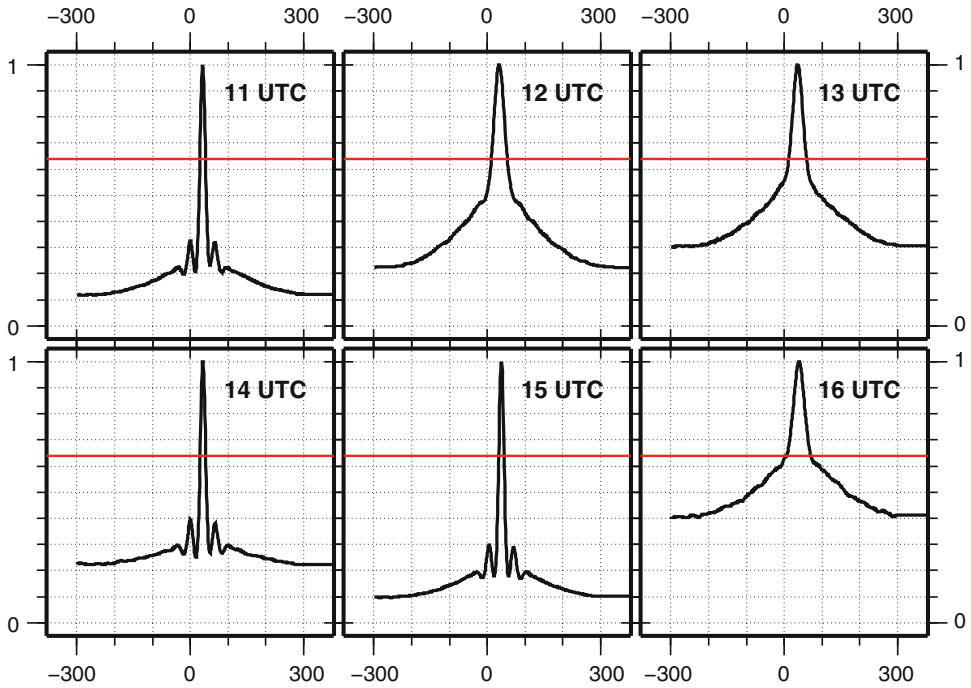

Fig. 4 Six normalized waveforms as a function of the correlator delay τ with the interval [−300:350]. These waveforms have been extracted from the data set obtained in Session B. The corresponding UTC epoch is indicated in each panel. Each waveform is the superposition of the codes present in the correlated signals. Near 11 UTC, 14 UTC and 15 h UTC there were M-code signals in addition to the C/A and P(Y) components. Because the C/A code contribution extends ±300 around the peak, the last values at the *right* end of each waveform could be taken as the noise to signal power. The changes in the relative noise level are partly because the transmitters had changing angular distances to the antennas' boresight. The *red line* corresponds to a relative power equal to 0.64 of the peak power, used to characterize the waveform width β. Note the apparent reduction in β and the increase in the SNR when the M-codes are present, implying a substantial increase in delay resolution

b and the desired calibrated delay observable τ^{PIR} using the equations:

$$\tau^{\mathrm{PIR}} = 0.5\left(\tau^{\mathrm{PIR}}_{\mathrm{rd}} - \tau^{\mathrm{PIR}}_{\mathrm{dr}}\right) \tag{7a}$$

$$b = 0.5\left(\tau^{\mathrm{PIR}}_{\mathrm{rd}} + \tau^{\mathrm{PIR}}_{\mathrm{dr}}\right) \tag{7b}$$

The main sources for the observed variations of $\tau^{\mathrm{PIR}}(t)$ are the mean sea level and the relatively faster changes in the positions of the contributing transmitters, as confirmed by the changes in $w^{\max}$ and β (Fig. 5, Panels 2 and 4). The variability of $\tau^{\mathrm{PIR}}(t)$ at shorter scales (min) is noise-like. The instrumental bias b corresponds to the differential instrumental delay between the signal paths from the switch to the signal processor, including the downconversion chains (Fig. 2). The variability of b has been estimated for the three intervals in which the width β of the waveform was smaller and stable. The results are given in Table 2:

GNSS-Ri altimetry model

As noted in the previous section, the GNSS-Ri observables are not assigned unambiguously to a particular satellite. In the GNSS-R applications, where a single transmitter is involved, the following expression is used, which relates the observable τ_S, the altimetric parameter H, and the elevation el^S of the observed satellite:

$$\tau_S = -2 \cdot H \cdot \sin(el^S) + n_\tau + n_{\mathrm{model}} \tag{8}$$

This includes measurement n_τ and model noise n_{model} terms. Additional terms accounting for differential tropospheric, ionospheric delays are negligible because of the proximity of the antennas to the sea surface. Due the smallness of the SWH, the effects of sea roughness have also been neglected. Because the range of el^S is reduced, the different parameters will show highly correlated effects with instrumental biases (Rius et al. 2010) and the use of this equation to obtain H requires additional information. The purpose now is to derive a generalization of Eq. 8 applicable to our GNSS-Ri observables.

We assume that, as a first approximation, each waveform around its peak could be described as a parabola. Assuming the validity of Eq. 6, Eq. 4 will read:

$$w_s = \sum_{\text{all } S} C^S \cdot (\tau - \tau_S)^2 \tag{9}$$

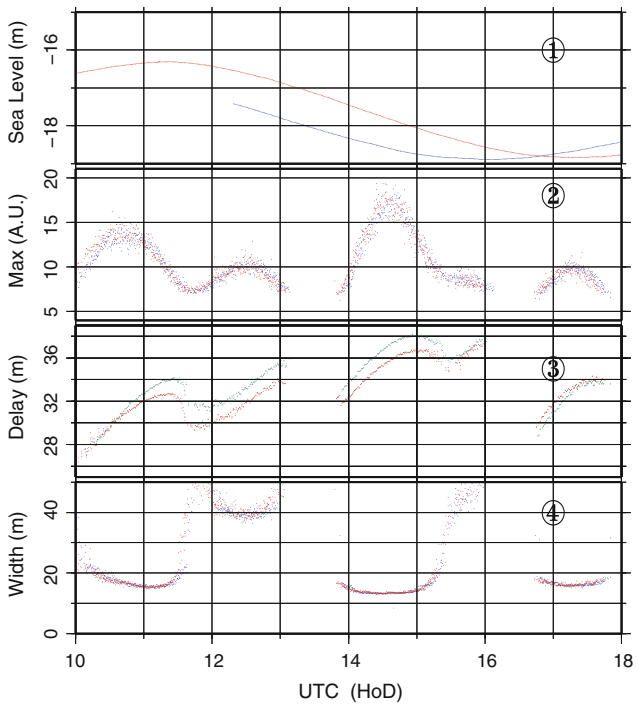

Fig. 5 Observable quantities obtained in both sessions. *Blue dots* correspond to Session A, and red dots refer to Session B. *Panel 1* contains the XBRA average mean sea level $H10$, referenced to the GNSS-Ri instrument. The remainder gives observable quantities extracted from the waveforms w_{dr}. *Panel 2* represents the observed waveform maximum power $w^{\max}$. *Panel 3* represents the delays τ^{pointing}. In the same panel, we have over plotted the delays τ^{peak} in *green* and *brown* for Sessions A and B respectively, showing that, within the noise, $\tau^{\mathrm{peak}} = \tau^{\mathrm{pointing}}$. *Panel 4* gives the waveform width $\beta(t)$

Table 2 Instrumental differential bias b mean and standard deviation computed for three intervals during Session B

Interval (hours UTC)	Bias b (m)	SD of b (m)
10.3–11.4	3.64	0.06
14.0–15.0	3.59	0.04
16.9–17.7	3.61	0.08

where

$$\tau_S = -2 \cdot H^{\mathrm{PIR}} \cdot \sin(el^S)$$

A relation between the delay of the maximum of the waveform τ_{PIR} and the height using PIR data H^{PIR} is easy to deduce, using a derivative of Eq. 9 at $\tau = \tau_{\mathrm{PIR}}$ of zero, and Eq. 8:

$$\tau^{\mathrm{PIR}} = -2 \cdot H^{\mathrm{PIR}} \cdot \sum_{\mathrm{all}\,S} c^S \cdot \sin(el^S) + n_\tau + n_{\mathrm{model}} \qquad (10)$$

where $c^S = C^S / \sum_{\mathrm{all}\,S} C^S$ are the normalized weights, and, as before, we have included terms to account for the measurement noise n_τ and the model noise n_{model}. This model noise term will depend mainly on the direction of the satellites, with a period of 1 sidereal day in a first approximation. Ignoring the noise terms, Eq. 10 could be used to obtain

$$H^{\mathrm{PIR}} = -\tau^{\mathrm{PIR}} \Big/ \left(2 \cdot \sum_{\mathrm{all}\,S} c^S \cdot \sin(el^S) \right)$$

In the computation of the weights c^S, see Eq. 6, we have assumed that the transmitter parameters P_T^S and G_T^S have common values for all satellites S and $G_{R,\mathrm{d}}^S$ and $G_{R,\mathrm{r}}^S$ have been computed assuming that the beam of both U and D antennas have a Gaussian pattern half-power beamwidth equal to 30°.

In Table 3, we indicate, for each GPS satellite above 15°, its PRN number, its launch year, approximate values of its a priori reflected to direct relative delay τ_{app}, elevation el^S and the normalized weights c_S at the start and end times of slices A and B.

After the experiment was performed, we noticed that on May 28 2010, a few days before our experiment, Block IIF SV with PRN 25 was launched and positioned in the same orbit and slot as Block IIR SV with PRN12. Both satellites were transmitting M-code signals. According to Table 3, during slices A and B, the relative delays between PRN 12 and PRN 15 changed between +1.4 and −0.3 m. Because the differences between the relative delays were smaller than the width of the autocorrelation of the code and their angular separation was smaller than the antenna beamwidth, we have applied the model given in Eq. 10 to this *double source*.

Comparison of GNSS-Ri and XBRA height estimates

In order to compare the results obtained, we will use the single and double-difference operators defined as

$$\Delta H(t) = H^{\mathrm{PIR}}(t) - H10(t) \qquad (11a)$$

Table 3 Satellites observed during slices A and B. We show for each satellite, block type, and launch year with approximate a priori relative differential delays in meters, elevations *el* in degrees, and weights for the start and stop times of slices A and B

Space vehicle			14:00 UTC			15:00 UTC		
PRN	Block	Year	τ_{app}	el	c_S	τ_{app}	el	c_S
9	IIA	1993	31.4	67	0.00	21.5	39	0.00
12	IIR	2006	31.6	68	0.81	33.7	83	0.18
14	IIR	2000	17.4	30	0.00	24.0	45	0.01
25	IIF	2010	30.2	63	0.19	34.0	87	0.75
27	IIA	1992	28.7	57	0.00	17.9	32	0.00
30	IIA	1996	17.2	30	0.00	28.3	56	0.06

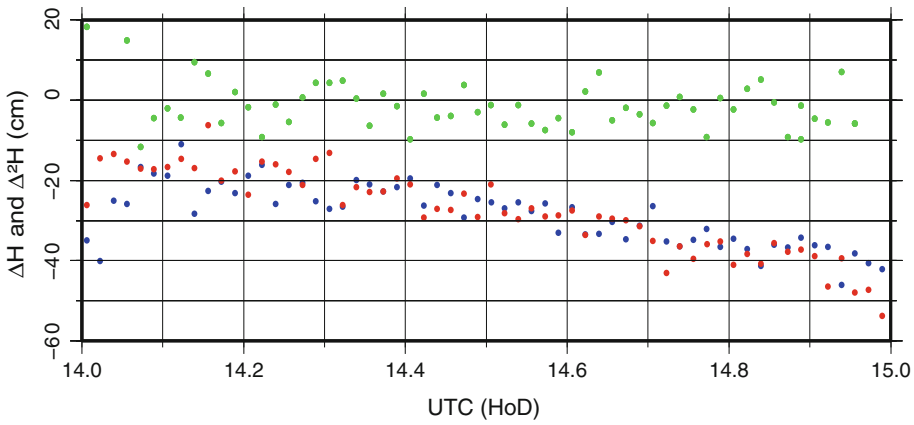

Fig. 6 Variation of the single-difference $\Delta H(t)$ for both slices. *Blue dots* indicate Slice A, and *red* refer to Slice B. The values of the double-difference $\Delta^2 H(t)$ are represented with *green dots*

$$\Delta^2 H(t) = \Delta H(t + 1 \text{ Sidereal Day}) - \Delta H(t) \tag{11b}$$

where $H10(t)$ is the 10-min average sea level height measured by the XBRA.

The single difference will provide a measure of the goodness of our model, and the double difference should cancel model uncertainties, in order for the precision of the method to be determined. Figure 6 shows $\Delta H(t)$ and $\Delta^2 H(t)$ computed with the data obtained in slices A and B. The series of single differences indicates that there is a bias and a linear variation, and the series of double differences does not show significant differences.

We have found from $\Delta^2 H(t)$ in the interval 14:10–14:30 UTC that its mean and standard deviation were $\langle \Delta^2 H \rangle = -1.5\,\text{cm}$ and $\sigma_{\Delta^2 H} = 3.6\,\text{cm}$, or $\sqrt{10} \cdot 3.6 = 11.4$ cm if we reduce the integration time from 10 to 1 s. From Eq. 11a, we could derive $\sigma_{H^{\text{PIR}}} = \sqrt{\sigma^2_{\Delta^2 H} \big/ 2 - \sigma^2_{H10}} = \sqrt{(11.4)^2 \big/ 2 - 2.9^2} = 7.5\,\text{cm}$, where we have used for σ_{H10} a value of 2.9 cm, which is the standard deviation of the XBRA data normalized to 1 s as already shown in the X-band radar altimeter section.

Conclusions

The first GNSS-R interferometric altimetry experiment yielded a 7.5 cm uncertainty in 1 s measurements, despite the nonoptimal conditions of the experiment, driven by the static and low-altitude position of the receiver. These conditions introduced contamination of the altimetric observables by simultaneous reception of multiple satellite signals, with different delays, and difficulties in properly modeling and correcting this effect. Nevertheless, these results are a significant improvement in signal envelope-based GNSS-R altimetric performance with respect to the standard C/A code correlation approach, which is in the order of 1 m (Spilker 1996), and still improvable under other more realistic observation geometries that permit delay-Doppler filtering of the different satellite contributions.

The results of this experiment consolidate the interferometric processing as the baseline for a demonstration space mission. In an orbital scenario, other factors not present in the bridge experiment will tend to degrade the performance, mainly the larger free-space loss of the reflected path, the increased roughness of the ocean surface, and the ionospheric and tropospheric delays. Larger antennas are needed for an experiment from space, of the order of 1 m^2, as well as careful compensation of the delay and Doppler shifts between the direct and reflected signals. On the other hand, the greater delay-Doppler separation between different GNSS satellites from orbital altitude will help discriminate different signals from different space vehicles, something that was not possible from the bridge.

Acknowledgments The X Band WaveGuide radar altimeter was kindly provided to us by RADAC BV, The Netherlands. We also would like to thank Tom van der Vlucht (RADAC), for his help with the bridge measurements, and the Province of Zeeland for permission to use the bridge. This research was supported by the European Space Agency (RFQ/3-127-47/09/NL/JD) and the Spanish Ministry of Science and Innovation (AYA2008-05906-C02-01/02). E.C. belongs to the Spanish *Ramón y Cajal* Program.

References

Barker BC, Betz JW, Clark JE, Correia JT, Gillis JT, Lazar S, Rehborn KA, Straton JR (2000) Overview of the GPS M code signal. In: Proceedings of the 2000 National Technical Meeting of the Institute of Navigation, Anaheim, CA, Jan 2000, pp 542–549

Garrison JL, Komjathy A, Zavorotny VU, Katzberg SJ (2002) Wind speed measurement using forward scattered GPS signals. IEEE Geosci Remote Sens 40(1):50–65

Gleason S, Hodgart S, Sun Y, Gommenginger C, Mackin S, Adjrad M, Unwin M (2005) Detection and processing of bistatically reflected GPS signals from low earth orbit for the purpose of ocean remote sensing. IEEE Geosci Remote Sens 43(6):1229–1241

Lowe ST, LaBrecque JL, Zuffada C, Romans LJ, Young LE, Hajj GA (2002) First Spaceborne observation of an Earth-reflected GPS signal. Radio Sci 37(1):7-1–7-28

Martín-Neira M (1993) A passive reflectometry and interferometry system (PARIS): application to ocean altimetry. ESA J 17: 331–355

Martín-Neira M, D'Addio S, Buck C, Floury N, Prieto-Cerdeira R (2011, in press) The PARIS ocean altimeter in-orbit demonstrator. IEEE Trans Geosci Remote Sens

Rius A, Cardellach E, Martín-Neira M (2010) Altimetric analysis of the sea-surface GPS-reflected signals. IEEE Trans Geosci Remote Sens 48(4):2119–2127

Spilker JJ (1996) GPS Signal structure and theoretical performance. In: Parkinson BW, Spilker JJ (eds) Global Positioning System: Theory and Applications, American Institute of Aeronautics, Vol I, Washington, DC

Thompson AR, Moran JM, Swenson GW (2004) Interferometry and synthesis in radio astronomy, 2nd edn. Wiley, New York

Wong G, Phelts RE, Walter T, Enge P (2010) Characterization of signal deformations for GPS and WAAS satellites. Institute of Navigation, Global Navigation Satellite Systems Conference, Portland

Zavorotny VU, Voronovich AG (2000) Scattering of GPS signals from the ocean with wind remote sensing application. IEEE Geosci Remote Sens 38(2):951–964

Author Biographies

Antonio Rius received the Ph.D. degree in astrophysics from Barcelona University, Barcelona, Spain, in 1974. From 1975 to 1985, he was a Member of the Technical Staff at NASA's Deep Space Communications Complex, Madrid, Spain, where he was responsible for the radio astronomical activities. Since 1986, he has been with the Spanish Consejo Superior de Investigaciones Científicas, Barcelona. He is currently responsible for the research group on Earth Observation at the Institut d'Estudis Espacials de Catalunya (IEEC). His current research interests include applications to Earth Science of the Global Navigation Satellite Systems.

Oleguer Nogués-Correig received the M.Sc. degree in telecommunication engineering from the Universitat Politcnica de Catalunya (UPC) on Nov 2002. From Jul 2000 to Mar 2001, he worked as antenna design engineer for mobile applications at the Spanish firm FRACTUS S.A. From Sep 2001 to Sep 2002 he joined the Elctromagnetics and Photonics Engineering Group at UPC, and since Dec 2002 he has been at the Institut d'Estudis Espacials de Catalunya (IEEC). His research interests since 2001 include the design and development of new GNSS-R observation instruments, with applications to the Earth Science.

Serni Ribó received the M.S. degree in telecommunication engineering in 1999 and PhD. degree in 2005 from the Universitat Politécnica de Catalunya, Catalonia, Spain. In 2000, he joined the European Space Agency (ESA), with a grant from the Spanish Ministry for Science and Technology, were he worked with synthetic aperture radiometry technology aspects. Since 2003 he is with the Space Research Institute of Catalonia .

Estel Cardellach received a PhD degree from the Polytechnic University of Catalonia, Barcelona, Spain, in 2002. She has been working on scientific applications of GNSS for remote sensing of the Earth, such as extraction of geophysical information of the GNSS reflected signals, radio occultation, and geodetic techniques. She was a National Research Council Awardee for a postdoctoral position at NASA/Jet Propulsion Laboratory, Pasadena, CA (2002-2003); a postdoctoral researcher at Harvard Smithsonian Center for Astrophysics, Cambridge, MA (2003-2005). Since 2005 she is at the Institute of Space Sciences (ICE-CSIC/IEEC), currently under the Spanish Ramón y Cajal program.

Santi Oliveras received the M.Sc. degree in telecommunication engineering from the Polytechnic University of Catalonia (UPC), Catalonia, Spain, in 2002. In 2007 he obtained a software engineering master from the UPC Foundation. From October 2002 to March 2004 he worked in Neotech Comunicacions S.L. selling technological. Since April 2004, he has been a member of the Earth Observation group at the Institut de Ciències de l'Espai, Institut d'Estudis Espacials de Catalunya (CSIC-IEEC). His current research interests include web and GNSS software applications to Earth science of GNSS.

Enric Valencia was born in 1982 in Sabadell, Catalunya. He received the degree and master in Electronic Engineering from the Universitat Politécnica de Catalunya (UPC) in April 2007, and after that he joined the Passive Remote Sensing Group of the Signal Theory and Communications (TSC) department of the UPC. His current research activities involve the use of different Global Navigation Satellite Signals Reflectometry (GNSS-R) techniques in order to retrieve geophysical parameters from ocean and land surfaces, as sea state or soil moisture, using simulators and developing instrumentation.

Hyuk Park was born in South Korea. He received the B.S. degree in mechanical engineering from Korea Advanced Institute of Science and Technology (KAIST) in 2001, and received the M.S. and Ph.D. degree in information and mechatronics from Gwangju Institute of Science and Technology (GIST), Korea, in 2003 and 2009, respectively. His main research interest is in the area of remote sensing, especially passive microwave remote sensing, including system design, modeling and simulation, and data / image processing. In 2009, he joined the remote sensing group of the Polytechnic University of Catalonia (UPC), Barcelona, as a postdoctoral researcher. Currently, he is working with the passive remote sensing group in the UPC for satellite remote sensing for microwave radiometry and GNSS-R.

José Miguel Tarongí was born in Palma de Mallorca, Spain. He received the degree in Telecommunication Engineering from the Universitat Politècnica de Catalunya (UPC) in Feb 2006. He joined the Pasive Remote Sensing Group of the Signal Theory and Communications (TSC) department of the UPC in Sep 2006. His primary areas of research include K band real aperture radiometry, the design of a multiband real aperture radiometer and the study of the radiofrecuency interference cancellation.

Adriano Camps received the degree in Telecommunications Engineering and Ph.D. degree in Telecommunications Engineering from the Universitat Politècnica de Catalunya (UPC), Barcelona, Spain, in 1992 and 1996. He has been with the Department of Signal Theory and Communications, UPC, as Assistant Profesor (1993-1997), as Associate Professor (1997-2007), and as Full Professor (2007-present). His research interests are focused in microwave remote sensing, mainly in microwave radiometry by aperture synthesis techniques (ESA's SMOS Mission) and remote sensing using signals of opportunity (GNSS-R).

Hans van der Marel is assistant professor at the Delft University of Technology, faculty of Aerospace Engineering. He has a background in geodesy and astrometry. He has been involved in GNSS applications since 1989, including high precision navigation, positioning and atmospheric remote sensing.

Roel van Bree graduated in Astronomy from Leiden University in the Netherlands in 1997. He has worked for ten years at TNO Defense and Security on Synthetic Aperture Radar. Currently, he is working as a research associate at Delft University of Technology on precise point positioning and navigation with GPS and Galileo.

Bas Altena is a M.Sc. student Geomatics at the Delft University of Technology, the Netherlands. He received his B.Sc. in Geodesy from the Hogeschool Utrecht, the Netherlands. His research interest focusses on the use of geodetic applications in geosciences.

Manuel Martín-Neira received the M.S. and Ph.D. degrees in telecommunication engineering in 1986 and 1996 respectively from the School of Telecommunication Engineering, Polytechnic University of Catalonia, Spain. From 1989 to 1992 he joined GMV, a Spanish aerospace company. Since 1992, with ESA working on aperture synthesis radiometry and on the PARIS concept for the use of GNSS signals reflected from the ocean. He is Confirmed Inventor from ESA, received the Salva i Campillo Award and the Premio Jaime I in 2010 from Spain, and is member of the Academie des Technologies of France.